A carbonaceous chondrite and cometary origin for icy moons of Jupiter and Saturn

Bruno Reynard, Adrien Néri, François Guyot, Christophe Sotin

To cite this version:

Bruno Reynard, Adrien Néri, François Guyot, Christophe Sotin. A carbonaceous chondrite and cometary origin for icy moons of Jupiter and Saturn. Earth and Planetary Science Letters, 2020, 530, pp.115920. 10.1016/j.epsl.2019.115920 . hal-02985826

HAL Id: hal-02985826
https://hal.science/hal-02985826v1

Submitted on 21 Dec 2021

A carbonaceous chondrite and cometary origin for icy moons of Jupiter and Saturn

Adrien Néri[1§], François Guyot[2], Bruno Reynard[1*], Christophe Sotin[3]

[1]University of Lyon, ENS de Lyon, CNRS, Lyon, France

[2]Museum National d'Histoire Naturelle, Sorbonne Université, IMPMC, UMR CNRS 7590, IRD UMR206, Paris, France

[3]Jet Propulsion Laboratory-California Institute of Technology, Pasadena, CA, USA

[*]Corresponding author: bruno.reynard@ens-lyon.fr

[§]Present address: IRAP, Université de Toulouse, CNRS, CNES, UPS, (Toulouse), France

Abstract

The inner structure of icy moons comprises ices, liquid water, a silicate rocky core and sometimes an inner metallic core depending on thermal evolution and differentiation. Mineralogy and density models for the silicate part of the icy satellites cores were assessed assuming a carbonaceous chondritic (CI) bulk composition and using a free-energy minimization code and experiments. Densities of other components, solid and liquid sulfides, carbonaceous matter, were evaluated from available equations of state. Model densities for silicates are larger than assessed from magnesian terrestrial minerals, by 200 to 600 kg.m^{-3} for the hydrated silicates, and 300 to 500 kg.m^{-3} for the dry silicates, due to the high iron bulk concentration in CI. The stability of Na-phlogopite in the silicate fraction up to 1300K favors the trapping of most ^{40}K in the rocky/carbonaceous cores with important consequences for modeling of the thermal evolution of icy satellites. We find that CI density models of icy satellite cores taking into account only the silicate and metal/sulfide fraction cannot account for the observed densities and reduced moment of inertia of Titan and Ganymede without adding a lower density component. We propose that this low-density component is carbonaceous matter derived from insoluble organic matter, in proportion of ~30-40% in volume and 15-20% in mass. This proportion is compatible with contributions from CI and comets, making these primitive bodies including their carbonaceous matter component likely precursors of icy moons, and potentially of most of the objects formed behind the snow line of the solar system.

Keywords: satellite, core composition, Titan, Ganymede, comet, carbonaceous chondrites

1. Introduction

Icy satellites are poorly known bodies, with Jupiter's Ganymede and Callisto, and Saturn's Titan the largest ones, similar in size to Mercury (with radii R > 2400 km) but with much lower mass M and mean densities of 1800-2000 kg.m^{-3} consistent with assemblages of ice and rock in various ratios (Anderson et al., 1996; Anderson et al., 1998). Their reduced moments of Inertia (MoI=C/MR^2, equal to 2/5 for homogeneous sphere where C is the average moment of inertia relative to the spin axis) differ significantly from 0.311 for differentiated Ganymede to ~0.355 for the least differentiated Callisto, respectively, Titan being at an intermediate stage of differentiation with a value of 0.3414. We focus here on the largest icy satellites, Callisto, Ganymede and Titan, and will not discuss the case of Io, which is totally dehydrated due to high temperatures and volcanic activity, or of smaller Europa.

Although quite similar in size and density, Callisto, Ganymede and Titan have different structures. Callisto and Ganymede present salty internal oceans whose presence is inferred from the magnetic fields induced by the Jovian environmental plasma (Kivelson et al., 1996; Kivelson et al., 2002; Zimmer et al., 2000), and similar conclusions were reached for Titan around Saturn from gravity and radar observations (Baland et al., 2011; Iess et al., 2012). For Ganymede, the presence of an inner metallic core was inferred from detailed analysis of its magnetic field (Anderson et al., 1996; Kivelson et al., 2002), a sign of a high degree of differentiation in agreement with the low MoI. The internal structure of these satellites is usually described as stratified layers composed of liquid iron sulfide alloy (only for Ganymede), silicates and iron sulfide mixture, and of ice and liquid water from the innermost to the outermost shells.

Titan's internal structure models match observations with four layers, assuming hydrated silicate core mineralogy (Castillo-Rogez and Lunine, 2010; Fortes, 2012) surrounded by a high-pressure ice layer, an ocean, and an ice crust (Baland et al., 2011; Iess et al., 2012). Titan's surface is active with ice mountains, hydrocarbon lakes (Lellouch et al., 2004; Stofan et al., 2007), and methane atmosphere indicative of internal activity (Tobie et al., 2006). Callisto is considered as not or only partially differentiated (Mueller and McKinnon, 1988), and surface features do not indicate significant internal activity (Schubert et al., 1981). Its MoI of 0.3549(42) if hydrostaticity is assumed, but if this assumption is not verified, the range of possibilities is large for its internal rocky core (Anderson et al., 2001). We therefore considered only the case of Titan where MoI is determined from a larger number of flybys for the low-temperature satellites.

Ganymede's internal structure models assume at least five layers (Mueller and McKinnon, 1988; Schubert et al., 1996; Vance et al., 2014) with an iron-rich core at the center, between 1/4 and 1/3 of the radius depending on sulfur content (Sohl et al., 2002). Silicate layers surrounding this metallic core have a mineralogy that is dominated by dry silicate mantle, or by mixed dry/hydrous minerals depending on the thermal model (Scott et al., 2002). A hydrosphere layer including a ocean sandwiched between a high-pressure ice layer and the outer ice crust surrounds the silicate-metal core (Grasset et al., 2013).

Internal structure and density models are usually based on the assumption that mineralogy includes only silicates and iron sulfides, and neglect carbonaceous matter present in primitive material like CI chondrites. Densities of Mg-rich terrestrial hydrated minerals are used for Titan (Fortes, 2012), while realistic compositions for the icy satellites are likely more iron-rich (Bland et al., 2004). If iron concentration is a free parameter, it leads to non-chondritic Fe/Si ratios (Sohl et al., 2002) as it may enter silicates in larger amounts than on Earth. No formation model accounts for large variations of the Fe/Si ratio inferred in Jovian satellites (Sohl et al., 2002), nor for the hydrous Mg-silicate composition required for matching the density and MoI of Titan. Therefore, instead of leaving bulk composition as a free parameter with resulting variations not accounted for by known cosmochemical or mechanical segregation mechanisms, we chose here to assume a common composition for the precursors of the rocky cores of icy satellites.

We assume a CI carbonaceous chondrite composition for the interiors of icy satellites (Mueller and McKinnon, 1988), *i.e.* essentially a solar composition except for H, He and the most volatile components (Lodders, 2003; Wasson and Kallemeyn, 1988), as a common origin for objects formed mainly beyond the snow line in the solar system. With this hypothesis, mineral compositions, metal-sulfide-silicates cannot be varied independently other than by assuming different evolution, in particular the segregation of an inner metallic core. Silicate mineralogy and density profiles in the icy moons are computed using the thermodynamic software Perple_X (Connolly, 1990) at relevant pressures and temperatures. Preliminary high pressure and temperature experiments are used to check the reliability of the thermodynamic calculations in iron-rich chondritic compositions of hydrous silicates. Evolution of organic precursors with bulk chondritic CI composition and their reactivity with silicates and sulfides were evaluated.

Two structural models are built for Titan and Ganymede depending on the degree of differentiation, resulting in different iron contents in the silicate fraction. Density and MoI models are constructed with available equations of state of the three main core components, silicates, iron sulfide and its liquid alloys, and carbonaceous matter derived from insoluble organic matter (IOM) of CI or comets. Carbonaceous matter proves to be an essential component for matching density and MoI of the satellites, and is likely derived from cometary nuclei precursors.

2. Compositional model

CI carbonaceous chondrite composition (Wasson and Kallemeyn, 1988), similar to that of the solar photosphere (except for volatile elements), was assumed to represent that of the solar nebula and other primitive objects like comets and interplanetary dust particles, providing the potential primordial material for formation of dwarf planets, satellites, and trans-Neptunian objects (TNO) beyond the snow line (McKinnon et al., 2017; Mueller and McKinnon, 1988).

Composition was simplified to major elements O, Fe, Mg, Si, S, Al, Ca, Na (98 wt%) to perform thermodynamic calculations and experiments in the silicate subsystem. Minor elements manganese, nickel and chromium (summing to ~1.5wt%) easily substitute to iron into crystalline structures, and were added to the Fe component ("Fe" = Fe + Mn + Ni + Cr). Sodium (~0.5%) and potassium (~0.05wt%) also substitute each other in minerals, and the formation of soluble salts (NaCl and KCl) with chlorine is assumed, which were subtracted from the "Na" component ("Na" = Na + K – Cl). This accounts for 99.5wt% of the silicates, and trace elements (~0.5% of the composition) were neglected (Table 1). Slightly different average CI compositions could be used (Lodders, 2003), with differences between CI compositions being mainly the sulfur content.

From this initial composition, two scenarios of evolution are considered that will result in different compositions of the rocky cores of icy satellites (Table 1). In model 1, the rocky core is not differentiated, the temperature remained low enough to avoid sulfide-silicate separation, the composition of the rock is homogeneous, and identical to that of CI chondrites. In model 2, the rocky core is differentiated and an inner metallic core segregated in the liquid state assuming a Fe-FeS eutectic composition (Fei et al., 1997), because segregation takes place as soon as melting occurs. The resulting composition of the silicate fraction is that of CI chondrites from which more iron is subtracted than in model 1 to form an inner core with 25 wt.% S, corresponding to the eutectic composition at average pressure of about 4 GPa in the metallic core of Ganymede.

Carbonaceous and organic compounds containing C, H, N, O are an important component of CI, representing up to 4 wt% of the rock (Derenne and Robert, 2010). They are classically divided into soluble and insoluble organic matter (IOM), the latter representing about 75% of carbonaceous matter.

3. Methods

The open-access Perple_X software (Connolly, 1990), for which updates and benchmarks are regularly provided online http://www.perplex.ethz.ch/perplex_updates.html, was used to calculate the equilibrium mineral assemblages and compositions for a given bulk composition varying pressure and temperature. We used thermodynamic properties and solid solutions calibrated self-consistently on experiments and natural samples (Holland and Powell, 1998), with recent addition or antigorite serpentine (Padron-Navarta et al., 2013), and revised antigorite serpentine equation of state providing best agreement with high-pressure phase equilibrium data (Hilairet et al., 2006). Temperatures and pressures vary in the range 300-1300 K, 0.8-7 GPa, to cover conditions in icy satellites. Excess water is assumed (water activity fixed to 1) at all pressure-temperature (P-T) conditions to obtain the maximum stability of hydrated silicates during at the early stages of formation of satellites from a water-rich ice-rock mixture. Drier conditions would result in lowering the dehydration temperatures. Built files are given in supplementary material for reproduction of calculations.

FeS is assumed to be an independent component whose reaction with silicates is negligible. This is confirmed by experiments (see below) with only minor destabilization of troilite to form pyrrhotite, whose composition is close to that of troilite, coexisting with silicates. The silicate fraction composition is obtained by removing the troilite component (Table 1). Organic or carbonaceous matter is assumed to be a chemically independent system because it does not react significantly with silicates, at least at low temperatures (Scott et al., 2002). It is only assumed to maintain reducing conditions, so that ferric iron content is negligible in silicates. In CI chondrites, ferric iron occurs in the form of magnetite (Fe_3O_4), iddingsite and cronstedtite (Hyman and Rowe, 1983; King et al., 2015), as a result of alteration at low temperatures (<100°C). These near surface conditions on CI parent bodies are not met in the core of icy satellites, and mineralogy has to be reevaluated with thermodynamic and experimental modeling. Organic compounds may react with silicates at temperatures above 1000K, but there are too little experimental data thus far to quantitatively assess this possibility (Scott et al., 2002).

Perple_X has been calibrated on laboratory experiments that were carried out at temperatures as low 500-600K in fluid saturated conditions akin to those studied here. Perple_X provides accurate phase relations that are compatible with observations in natural rocks from cold subduction settings, and some of the thermodynamic data (Padron-Navarta et al., 2013) and phase relations used here have been tested on natural low-temperature serpentines that were formed over periods of a few to a few tens million years. Kinetic experiments also point to fast reactions at the geological timescale in the 500-900K temperature range when hydrated Mg-rich minerals (serpentines) and fluids are involved (Malvoisin et al., 2012). It is therefore reasonable to assume that equilibrium is reached to some extent even in the cold rocky core of Titan (Castillo-Rogez and Lunine, 2010) with reactive Fe-rich composition and longer timescales.

Since the database used in Perple_X is calibrated on terrestrial samples, it is desirable to check whether the extrapolation to extraterrestrial material compositions is accurate. Three preliminary experiments were performed to complement earlier work (Scott et al., 2002), in order to validate the consistency of the thermodynamic modeling. A starting material was synthesized by mixing oxide powders in the proportions given in the undifferentiated model (Table 1), minus FeO and FeS. The mixture was finely ground in an agate mortar, and held for one hour at 1650 °C in a platinum crucible, quenched, and the procedure repeated. Raman spectroscopy, scanning electron microscopy (SEM) and energy dispersive X-ray spectroscopy (EDX) mapping showed a chemically homogeneous, fine-grained mixture of olivine and pyroxene. Pieces of this material were finely crushed in an agate mortar in ethanol before each experiment for the high-pressure experiments. Iron was added under the form of troilite FeS and iron oxides, magnetite (Fe_3O_4) or wüstite (FeO), in proportions of the CI composition. Organic matter was added as an aliphatic chain (solid paraffin wax) and a soluble nitrogenous base (pyridine). The solid mixture was put into a gold capsule along with pyridine-water solution in proportions matching the N/C ratio of CI chondrites. Capsules are designed to seal in the press as pressure is increased. In order to ensure that the experimental load is saturated in water, diamond powder was added on top of the sample to create a non-reactive porous reservoir. The material was reacted for ~100 hours at a pressure of 1.5 GPa and temperatures of 773 and 873K in a belt apparatus. Hydrogen or H_2O losses are negligible at those conditions, and temperature is known to ±40K (Pilorgé et al. 2017). In the presence of excess sulfide or organic matter, it is assumed that the sample was self-buffered regarding the oxygen fugacity (Scott et al., 2002). At the end of each run, the capsules were opened along a longitudinal plane, trapped in epoxy resin and polished. They were analyzed using SEM, EDX, X-Ray Diffraction (XRD) and Raman spectroscopy. XRD showed only pyrrhotite-troilite solid solution, olivine and pyroxene, as well as gold and diamond from the capsule and trap. Raman spectroscopy was more efficient to detect minor newly formed phases.

4. Mineralogical and density calculations

4.1 Mineralogy of the different models

The difference of iron content has two major consequences on the phase diagram of the two models (Fig. 1). Dehydration occurs over a broader and lower temperature range in the iron-rich (model 1) than in the iron-poor silicates (model 2). Each diagram can be divided in three domains upon increasing temperature, firstly the region where mineralogy is dominated by hydrous minerals, secondly the dehydration region where hydrous minerals progressively decompose to form dry minerals, and thirdly the region where mineralogy is dominated by dry minerals.

The evolution of the amount of each phase for three isobars (fixed pressure and varying temperature) at 1.5, 3.0, and 4.5 GPa shows that the effect of pressure on the stability fields of minerals is relatively small over the studied range (Fig. 2). In the hydrated domain, mineralogy is dominated by hydrous phyllosilicates (layered clay-like minerals) chlorite, antigorite, and Na-rich phlogopite $(Na,K)Mg_3AlSi_3O_{10}(OH,F,Cl)_2$. Chlorite and antigorite, common Mg-rich hydrous minerals in hydrated basic to ultrabasic terrestrial rocks, contain ~ 12-13 wt.% H_2O, and Na-phlogopite, less common on Earth, contains ~ 4 wt.% of H_2O.

Na-phlogopite is important because potassium may substitute for sodium up to 1wt% in natural crystals (Schreyer et al., 1980), and it is stable up to 1300K. Thus it may trap all the available potassium into the rocky core, and control the early thermal history of the body when heat production was dominated by ^{40}K decay. Finally up to 20% amphibole with ~2.5 wt.% H_2O is formed at low pressures (<2.5 GPa), and remains stable up to high temperatures. Amphibole is an additional host for trapping potassium in the rocky core of icy satellites.

The difference in iron content between models does not significantly modify the nature of hydrous mineral phases, only their relative amount and composition. Depending on the iron content of the bulk rock, antigorite and chlorite behave differently. In model 1, the high amount of iron stabilizes a large amount of chlorite at the expense of antigorite, but their quantities reverse abruptly at ~ 520 K at nearly constant water content in the solid. In model 2, antigorite is the dominant phase over the whole hydrated assemblage stability field. This second model is similar to that of hydrated ultramafic rocks in terrestrial subduction zones (Padron-Navarta et al., 2013) with only slightly lower Mg number (Mg# = Mg/(Mg+Fe)) of ~0.87 instead of ~0.90 for common terrestrial peridotites.

From about 550 to 900K, the amount of dry minerals (e.g. olivine and pyroxene) increases at the expense of antigorite. The disappearance of antigorite is the leading reaction of dehydration: it has the strongest effect on the release of water because of high concentration (~12 wt.% H_2O) and high abundance. The effect of the iron content on dehydration is best seen when plotting the water content of the mineral assemblage in the rock against temperature (Fig. 3). In model 1, about 60 wt.% of hydrous minerals, chlorite and antigorite, with an iron-rich composition of the silicate fraction (bulk Mg# ~ 0.69) start to dehydrate around 550 K. This reaction is progressive up to ~820-870 K where the mineralogy is almost entirely dry, with only Na-phlogopite as a hydrous phase up to ~1150 K. In iron-poor model 2, antigorite destabilizes over a narrower and higher temperature range from 800 K to 920 K.

At high temperatures, the mineralogy is dominated by dry minerals olivine $(Mg,Fe)_2SiO_4$ and pyroxenes $Ca(Mg,Fe)Si_2O_6$ and $(Mg,Fe)_2Si_2O_6$. Na-phlogopite and amphiboles are the only hydrated minerals stable at temperatures higher than 900 K. The difference in composition between the two models does not change the nature of the dry mineral phases obtained from the thermodynamic model, only their relative amount and composition. In model 2, orthopyroxene and olivine are almost equally abundant and dominate the mineralogy. In the iron-rich composition M1, the proportion of olivine at high temperature is much higher than in model M2. Amphiboles are stable at low pressure and destabilize into garnet at higher pressure, around 3-3.5 GPa in M2, and 2.5-2.8 GPa in M1.

4.2 Comparison with experiments

XRD analysis of the experimental charges shows the presence of olivine and pyroxene in addition to products from the capsule and diamond trap, indicating that reaction with water was sluggish. This technique is unable to inform on the presence of a phase it is present in less than 5 % or has a low scattering factor. Raman spectroscopy analysis was conducted to detect minor phases. It revealed the presence of Na-phlogopite ($NaMg_3AlSi_3O_{10}(OH)_2$) (Fig. 4), one of the phyllosilicates predicted with Perple_X calculations. The absence of chlorite at 773 K is in agreement with the Perple_X predictions. The absence of antigorite suggests that our experiment was performed above the destabilization temperature of antigorite, within the error bar of the experiment (Fig. 2, M1 model).

Olivine and pyroxene are the major phases of the recovered samples, and are always enriched in Fe with respect to the Fe-free olivine and pyroxene of the starting material. No residual grains of the starting magnetite (Fe_3O_4) or wüstite (FeO) are recovered, as they dissolved into the silicate phases. Olivines adjacent to FeS precursor grains are enriched in iron from Fo_{81} for large patches of crystals to Fo_{32} in the most Fe-rich recrystallizations close to troilite grains partially transformed into pyrrhottite. Similar patterns of Fe-enrichment were observed on pyroxene grains near sulfide. Troilite reacted to form pyrrhotite ($Fe_{1-x}S$, $x<1/8$) identified by Raman and XRD, accounting for iron reduction in the oxide subsystem with a global reaction $FeS + x\ Fe_3O_4 = Fe_{1-x}S + 4x\ FeO$. The replacement of troilite (FeS) by pyrrhotite contributes to local (typically 10 micron scale) iron enrichment in the olivine and pyroxene, as a minor addition to iron oxide dissolution. This indicates that global dissolution of iron oxide in silicates took place, and that at least local equilibrium is reached at such low temperatures over the experiment duration.

Former experiments using CI starting composition (Scott et al., 2002) found that antigorite and chlorite are stable at low temperatures, in consistency with Perple_X predictions, but that talc forms at high temperatures, in contradiction with it. Identification of talc as dominant hydrous phases at high temperatures in their experiments relies partly on infrared (IR) spectroscopy. IR spectra only identifies vibrational modes associated with tetrahedral-octahedral-tetrahedral (TOT) layers of phyllosilicates that are common to talc and Na-phlogopite, with a possibly ambiguous determination. Raman spectroscopy allows unambiguous determination of the newly formed phyllosilicate as Na-phlogopite with characteristic Raman peaks including TOT and OH vibrations (Fig. 4), distinct from those of talc.

In spite of the need of further experimental effort to resolve potential issues with thermodynamic equilibrium and reaction between organic mater and silicates, the thermodynamic predictions from Perple_X are consistent with major features of experimental data indicating dominance of antigorite and chlorite at temperatures in the range 673-873K (Scott et al., 2002) and formation of Na-phlogopite at 773±40 K (this study).

Raman spectra of the organic matter show that initial components transformed into amorphous carbonaceous matter akin to IOM or coals (Quirico et al., 2009), as expected at 1.5 GPa and 773-873K (Chanyshev et al. 2017). This transformation occurs with partial loss of nitrogen, oxygen and hydrogen from the paraffin and pyridine precursors. The release of hydrogen may have buffered the oxidation state to ferrous iron, favoring dissolution of iron oxides in the silicates. Apart from buffering the oxidation state, no reaction between carbonaceous matter and silicates was observed. Potential reactions between silicates, sulfides and carbonaceous matter at temperature above 1000K (Scott et al., 2002) are not well documented and require further investigation.

4.3 Density profiles and equations of state of silicate-sulfide layers

From the mineral proportions and compositions, density models are computed using available equations of state in the Perple_X database. Silicate and oxide densities are known to within 1%. The density of the FeS phase is given by a Murnaghan equation of state:

$$\rho(\mathrm{P,T}) = \rho_0 \left[1 + P\left(\frac{K'_0}{K_0}\right)\right]^{1/K'_0} \left(1 - \alpha(T - T_0)\right) \tag{1}$$

with:

$$K_0 = K_0(T_0) + \left(\frac{\partial K_0}{\partial T}\right)_P (T - T_0) \tag{2}$$

where K_0 and K'_0 are the bulk modulus and its pressure derivative, respectively, and α the thermal expansivity. The density of the silicate – sulfide assemblage was calculated from volume conservation on mixing:

$$\rho_{mix} = \frac{\rho_{silicate}\rho_{FeS}}{\rho_{silicate}\omega_{FeS} + \rho_{FeS}\omega_{silicate}} \tag{3}$$

with ρ_{mix} the density of the rock-metal mixture, $\rho_{silicate}$ the density of the silicate predicted with model 1, ρ_{FeS} the density of the troilite phase (FeS), ω_{FeS} the mass fraction of the troilite in the rock-metal mixture, $\omega_{silicate}$ the mass fraction of the silicate in the rock-metal mixture. Parameters of equation (1) are T_0 = 1000K, K_0 = 54.3 GPa, K'_0 = 4, $\partial K_0/\partial T$ = -0.0117 GPa/K^{-1}, α = 1.042 10^{-4} K^{-1}, and ρ_0 = 4678 kg/m^3 (Urakawa et al., 2004). Pyrrhotite was not considered although it forms at the expense of troilite at low temperatures. Troilite was used as a proxy to pyrrhotite, whose equation of state is unknown, because of its similar composition and density, with an estimated uncertainty of 2%.

Assuming that the temperature of the core remained above the eutectic melting around 1225±10 K, average densities for the eutectic liquid with 25 wt% (or 37 mol%) S at 4 GPa are estimated as 5700±100 kg.m^{-3} (Morard et al., 2018). An inner core mass fraction of 35% is fixed by the eutectic and chondritic compositions (Table 1), yielding a radius fraction of 61.7% and volume fraction of 23.5 % for the inner liquid core. For the sake of MoI modeling, liquid densities were obtained by fitting third-order Birch-Murnaghan equation of state (Morard et al., 2018) for sulfur content X between 0 and 50 mol% to a simplified Murnaghan type equation of state similar to equation (1) with $\rho_{\square}(X)\square= 6950 - 5176\ X - 3108\ X^2$ in kg/m^3, T_0 = 1900K, $K_0(X) = 82.6^{(1-X)}\text{x}1.84^X$ GPa, K'_0 = 5.9, and α = 1.08 10^{-4} K^{-1}. The large composition range of the experimental data allows interpolation to the eutectic composition. The Murnaghan equation of state has the advantage of allowing direct calculation of density as a function of pressure over the Birch-Murnaghan equation of state.

Model 1 consists in a partially differentiated body, in which the hydrosphere was separated from the silicate-troilite assemblage forming a homogeneous rocky core with CI iron content in the silicate fraction. At temperatures below 900 K, the hydrated silicate assemblage has a density of ~3000 kg.m^{-3} (Fig. 5), which is higher than the estimations of ~2600-2700 kg.m^{-3} in previous studies for Titan (Castillo-Rogez and Lunine, 2010; Fortes, 2012), because of higher iron content in the present model. On increasing temperature, the density of the solids increases step by step due to the dehydration of various hydrous minerals until the temperature reaches ~900 K where density takes the steady value of the dry assemblage. When troilite is mechanically mixed with silicates, bulk density increases by about 300 kg.m^3 at 300 K and 220 kg.m^3 at 1300 K (green curve, Fig. 5a).

Model 2 represents a partially differentiated body, in which an inner core was formed with the composition of the Fe-FeS eutectic. The lower iron content of the silicate fraction for this model, Mg#=87 instead of 69 in model 1, results in lower densities (Fig. 5). The narrow dehydration zone results in a steep density increase in the 800-950 K range. At higher temperatures, density takes values of ~3150 to 3350 kg.m^{-3} depending on pressure from 1 to 5 GPa. Density increases by ~200 kg.m^{-3} over the whole pressure range, and a kink is observed around 3 GPa due to destabilization of Na-phlogopite and amphibole into garnet.

4.4 Density of carbonaceous matter

Carbonaceous matter is the third potential major component in CI composition metamorphosed to the conditions of icy satellite cores. There exist limited data on the density of such compounds, especially at high pressure, because they are mostly amorphous. Given the molecular complexity of IOM (Derenne and Robert, 2010), we estimated its density after thermal metamorphism assuming it is similar to that of carbonized coals (Franklin, 1949). Starting from values of 1300-1400 kg/m^3, coal density rises slowly to reach 1400-1500 kg/m^3 after heating to 873K before increasing abruptly to values of ~1800±100 kg/m^3 in the 1123-1373K range, finally raising slowly to ~2000-2100 kg/m^3 at 1900K, i.e. close to that of graphite (~2300 kg/m^3). Densities may vary with the origin of the coal, and the strong increase in density around 900 K is associated with loss of volatiles, mostly hydrogen (Franklin, 1949). Smoother increase above 1000K is attributed to increasing crystallinity. Decomposition of various complex organic molecules into amorphous carbonaceous matter and hydrogen occurs at temperatures of 800-900K, similar to hydrogen loss in coals. This carbonization temperature is insensitive to pressure up to 10 GPa (Chanyshev et al., 2017). We assume that similar compaction will occur with increasing temperature in the whole depth range of icy satellite cores. For the sake of simplicity, we assumed a density of 1400 kg/m^3 for temperature up to 900K, i. e. when silicate mineralogy is dominated by hydrous phases, and of 1800 kg/m^3 above, i. e. when dry silicates are formed, based on carbonized coals measurements (Franklin, 1949), taking into account an uncertainty of ±200 kg/m^3 in inferring the required fraction of carbonaceous matter.

5. Discussion

5.1 Mass-MoI relationship for CI silicate-sulfide models

To our knowledge, models of the density of icy satellites have thus far been built based on assemblages of ices and water, silicates and iron sulfur alloys. Other components were not explicitly considered in the calculation even though organic matter is mentioned in the composition of Titan's core (Fortes, 2012). We first test this hypothesis with the density profiles for the CI composition model for silicate-iron sulfide cores. This assumption determines the density profiles of the inner core and silicate layer, and their relative radii in model 2, and the silicate-sulfide proportion in model 1.

The temperature and density profiles in the hydrosphere for Ganymede are taken from the literature (Vance et al., 2014). The choice of the ice crust thickness is of second order in terms of the change in mass and MoI compared to the effect of iron on the density of the core. For Titan, the ice crust thickness is fixed at 76 km (Béghin et al., 2012), the temperature profile is conductive in the ice crust, adiabatic in the ocean and follows the melting curve in the high-pressure (HP) ice layer where the boundary with the ocean is a temperate layer (Kalousová and Sotin, 2018) at the melting temperature of ice. The temperature in the HP ice layer may be 10 to 20 K lower than the melting temperature, which results in a negligible density change. Heat transfer by conduction in the silicate shell is calculated using spherical solution of a volumetrically heated shell., and the density profile in the hydrosphere is computed using the equation of state for water and ice (Vance et al., 2014). The densities of the crust, ocean, and HP ice vary from 0.832 to 0.928, 1.046 to 1.2038, and 1.3377 to 1.3770, respectively. The gravity acceleration profile depends on the density profile, which is not known a priori. Therefore, we use an iterative process to determine the gravity acceleration. The process converges after the second iteration.

The internal structure of Ganymede consists of as much as five layers, an iron-rich liquid inner core, a silicate layer, a high-pressure ice layer, an ocean, and an ice crust (Anderson et al., 1996; Schubert et al., 1996). In order to segregate an inner metallic core, the melting temperature of the Fe-FeS eutectic has been reached through the whole volume of silicates, i. e. 1200-1300K (Fei et al., 1997). This is well above the dehydration temperature of major hydrous silicates (Figs. 1 and 2). The mean density of the silicate layer is taken as that of the nearly entirely dehydrated assemblages for model 2 (3250-3300 kg.m^{-3}), potential hydrous phases being limited to Na-phlogopite and amphibole stable above 900 K (Fig. 2). Beneath the hydrosphere, there might be a thin hydrated layer due to water rock interactions near the ice-silicate core interface surrounding the dry silicate layer, and the inner metallic core with the composition of the Fe-FeS eutectic (Fig. 6). For the sake of simplicity, the small hydrated silicate layer was not considered in modeling the mass-MoI relationship. As mentioned above, compositional constrains give a relative radius of 62.5 % for the metallic inner core. With an estimated ice thickness of 800 km (Vance et al., 2014), this gives a core radius of 1830 km and an inner metallic core radius of 1140 km, compatible with former estimates in the 650-1300 km range (Anderson et al., 1996).

With its MoI of 0.3414 (Iess et al., 2012), Titan is differentiated, but not as much as Ganymede. Inner temperatures are low (Fortes, 2012), there is no evidence of a metallic inner core, and model 1 is applied with a silicate-troilite core composed of hydrous silicates with an average density of ~3300 kg.m^{-3}. This high value is due to the high iron content in chondritic hydrous and anhydrous silicates with respect to terrestrial value commonly used in modeling of 2520-2670 kg.m^{-3} (Castillo-Rogez and Lunine, 2010; Fortes, 2012), and to the addition of troilite.

Integration of density profiles yields the relationship between MoI and mass for model 1 Titan and model 2 Ganymede (Fig. 7) within a fixed radius geometry and CI composition, and varying the depth of the high-pressure ice-core limit (Table 2). This is equivalent to varying the bulk water/rock ratio of the satellite. It is clear that none of the CI chondrite models taking into account only silicates and iron sulfides for the rocky cores can account for the observed values on Titan and Ganymede (Fig. 7). Considering non-hydrostaticity on Titan based on the presence of topographic depressions at the poles (Sotin et al., 2018) brings the MoI value closer to the mass-MoI relationship of the models but is far from solving the problem. Non-hydrostaticity on Ganymede cannot be determined as only one gravity coefficient was determined. One way to solve this issue is to reduce the density of the rocky cores by adding a low-density component to the CI chondrite silicate-sulfide assemblage, with IOM as a likely low-density candidate.

5.2 Carbonaceous matter as the required low density component

There exist several solutions to the issue raised in the previous section. A common one is to infer the density of minerals in the rocky core by assuming values measured on terrestrial samples. A typical example is serpentine for which zero pressure densities of 2500-2650 kg.m^{-3} are used (Castillo-Rogez and Lunine, 2010; Fortes, 2012). The composition of terrestrial serpentines is, however, very magnesian (Mg# = 90-93), whereas actual values in CI are iron-rich with a important cronstedtite component, and with additional magnetite (Bland et al., 2004). Assuming terrestrial serpentine composition is therefore not justified because it would require either strong chemical heterogeneities in the region of formation of icy moons, or strong partitioning of iron to a metallic inner core in a CI composition model, at temperatures incompatible with the stability of hydrous phases (model 2).

An alternative approach consists in relaxing the chondritic composition constrain, and varying major element ratios, in particular the Fe/Si ratio (Sohl et al., 2002). These authors found that Fe/Si ratios of the Jovian satellites have to be significantly superchondritic for Callisto and Ganymede, and chondritic to infrachondritic for Europe and Io in order to fit mass-MoI data with simplified mineralogical models. This hypothesis implies an unknown mechanism for building chemically distinct regions around Jupiter (Sohl et al., 2002). Assemblages of rock and ice have also been advocated to explain low densities in satellite cores, but keeping ice in icy moon cores may prove difficult because of heating and melting (Fortes, 2012).

As an alternative, we test the hypothesis that carbonaceous matter derived from IOM of CI chondrites provides the missing low-density phase required to match the MoI and mass observations for Titan and Ganymede. Carbonaceous matter has not been considered explicitly in former models of inner structure of icy moons, possibly because carbon is considered a volatile element especially when oxidized.

Carbonaceous matter, coals or IOM with relatively low heteroatom (H, O, N) contents turn out to be refractory phases by losing heteroatoms upon heating with a sharp density increase near 900K (Franklin, 1949), and resist thermal metamorphism in chondrites (Quirico et al., 2009). Crystals of large organic molecules transform to carbonaceous matter and hydrogen over a small temperature range of 800-900K at pressures encountered in icy satellites (Chanyshev et al., 2017). Also, the formation of carbonaceous matter is reported in terrestrial subduction metamorphism at temperature around 800-900K and pressure of 2-2.5 GPa (Vitale Brovarone et al., 2017). Thus formation of amorphous then graphitic carbon and finally graphite upon increasing temperature from organic precursors is the rule rather than the exception in experimental and natural systems, supporting the idea that carbonaceous matter was preserved during the formation and evolution of bodies as large as ~ 2500 km in radius. Carbon could also be incorporated in iron alloys to form Ganymede's inner core. Solubility data in complex Fe-S-Si-C composition suggest little carbon is incorporated in liquid metal at low pressure and temperature (Deng et al., 2013). It was thus assumed that the inner core is carbon-free.

As discussed earlier, we can distinguish three regions with specific densities of carbonaceous matter (Franklin, 1949). Firstly a low temperature region corresponding to that where hydrous silicates are stable, and the density of carbonaceous matter is ~1400 $kg.m^{-3}$ for application to Titan. Secondly a medium temperature region where silicates are mostly dry, where the density of carbonaceous matter is ~1800 $kg.m^{-3}$ for application to Ganymede. Using these values, we estimated the amount of carbonaceous matter by fixing the mass and radius to observed values, and using a mean density for the silicate and sulfide fractions of the core. Carbonaceous matter is added over the whole core in Titan, and only in the silicate portion in Ganymede (percentage is given below with respect to the whole mass of the rocky core, including silicate and metal). This second hypothesis has a small effect when compared with variability of carbonaceous matter densities (Franklin, 1949), estimated here by setting a large uncertainty of ±200 $kg.m^{-3}$. Taking into account uncertainties on silicate-sulfide assemblages and carbonaceous matter, and a 100 $kg.m^{-3}$ uncertainty on core density, Titan mass and MoI can be explained with CI chondrite composition by adding ~23±10 wt.% (or ~45% in volume) of carbonaceous matter (Fig. 7), and 17±10 wt.% (~30% volume) if the MoI is corrected for non-hydrostaticity estimated from the ellipticity of Titan shape (Sotin et al., 2018). A remarkably similar amount (16±10 wt.%) is required to bring the MoI of Ganymede to the observed value. This yields a molar C/Si ratio ~4±2.5. These results are much higher than the organic matter content of 4 wt.% in CI (Derenne and Robert, 2010), or C/Si~0.6-1 (Lodders, 2003), but consistent with the high concentration of organics and carbonaceous matter of comets (Bardyn et al., 2017; Fulle et al., 2016). Comets may represent an additional precursor to icy satellites, with mineral phases akin to those of chondrites (Brownlee et al., 2006) but higher organic matter concentrations (Bardyn et al., 2017; Fulle et al., 2016). Degassing of light hydrocarbons from this primitive material would be consistent with a primordial origin of Titan atmosphere (Mousis et al., 2009).

6. Conclusions

We have evaluated the consequences of chemical and mineralogical composition hypotheses on the internal structure of icy satellites. Within the carbonaceous chondrite composition model, mass and MoI of Ganymede, a hot and differentiated satellite with mostly dehydrated core, and of Titan, a cold and mildly differentiated satellite with mostly hydrated core, can be accounted for provided a low density component is added to classical models to compensate for the high-density of iron-bearing silicates.

This low-density component is refractory carbonaceous matter deriving from IOM of the CI chondrites or comets, in proportions that match observed concentrations of the latter. High organic contents have already been assumed in modeling of for the Pluto-Charon system (McKinnon et al., 2017) based on cometary precursor compositions (Bardyn et al., 2017; Fulle et al., 2016). More recently, it was found that Ceres surface would contain up to 20 wt% of organic matter (Marchi et al., 2019). Like the large icy moons Ganymede and Titan, a number of water rich bodies may have formed from a cosmochemical reservoir defined by high-organic-content comets and carbonaceous chondrites beyond the snow line of the solar system.

A second consequence of the CI composition model is that large amounts of ^{40}K can be stored in the rocky cores of icy satellites in Na-phlogopite and amphiboles, with important consequences on their thermal evolution and dynamics. Solid-state convection in the rocky core may be needed to extract excess heat, and conditions for establishing convection have to be assessed.

The conclusions reached here are based on the assumptions that carbonaceous matter and silicates/iron sulfide do not react, an hypothesis that seems valid up to moderate temperatures of ~900 K but may fail at higher temperatures where carbonate formation was observed (Scott et al., 2002).

The ESA JUICE mission to be launched in 2022 will orbit Ganymede to provide the degree 2 gravity coefficients with orders of magnitude better accuracy, higher degree gravity coefficients, higher degree magnetic coefficients, and time-dependent (tidal) topography. With these measurements, the thickness of the different layers, the non-hydrostatic effects and the values for the density of the ocean if it exists (Grasset et al., 2013) will be precisely determined. The JUICE mission will also perform a dozen flybys of Callisto, from which interior models will be constrained although not as well as for Ganymede.

Finally, the recently selected NASA New Frontiers 4 Dragonfly mission includes a seismometer (Lorenz et al., 2019) that will improve our knowledge of Titan’s interior structure. All these data will provide further tests for the presence of a large fraction of organic matter in the interior of the large icy moons.

Acknowledgments.

The large volume high-pressure experiments were performed at the PLECE Platform of the Université de Lyon with the help of Sylvie Le Floch, and Raman spectroscopy at ENS Lyon with the help of Gilles Montagnac. This work was supported by INSU through the national Raman facility in Lyon and PNP grant to BR. BR acknowledges the LABEX Lyon Institute of Origins (ANR-10-LABX-0066) of the Université de Lyon for its financial support within the program "Investissements d'Avenir" (ANR-11-IDEX-0007) of the French government operated by the National Research Agency (ANR). CS acknowledges support by the NASA Astrobiology Institute under Cooperative Agreement Notice NNN13D485T, "Habitability of Hydrocarbon Worlds: Titan and Beyond". Anonymous referees provided valuable comments that allowed improving the manuscript.

References

Anderson, J.D. et al., 2001. Shape, Mean Radius, Gravity Field, and Interior Structure of Callisto. Icarus, 153: 157-161.

Anderson, J.D., Lau, E.L., Sjorgren, W.L., Schubert, G., Moore, W.B., 1996. Gravitational constraints on the internal structure of Ganymede. Nature, 384: 541-543.

Anderson, J.D. et al., 1998. Distribution of rock, metals, and ices in Callisto. Science, 280: 1573-6.

Baland, R.M., Van Hoolst, T., Yseboodt, M., Karatekin, O., 2011. Titan's obliquity as evidence of a subsurface ocean? Astronomy & Astrophysics, 530: A141.

Bardyn, A. et al., 2017. Carbon-rich dust in comet 67P/Churyumov-Gerasimenko measured by COSIMA/Rosetta. Monthly Notices of the Royal Astronomical Society, 469: S712-S722.

Béghin, C. et al., 2012. Analytic theory of Titan’s Schumann resonance: Constraints on ionospheric conductivity and buried water ocean. Icarus, 218: 1028-1042.

Bland, P.A., Cressey, G., Menzies, O.N., 2004. Modal mineralogy of carbonaceous chondrites by X-ray diffraction and Mössbauer spectroscopy. Meteoritics & Planetary Science, 39: 3-16.

Brownlee, D. et al., 2006. Comet 81P/Wild 2 under a microscope. Science, 314: 1711-1716.

Castillo-Rogez, J.C., Lunine, J.I., 2010. Evolution of Titan's rocky core constrained by Cassini observations. Geophysical Research Letters, 37: L20205.

Chanyshev, A.D. et al., 2017. Transition from melting to carbonization of naphthalene, anthracene, pyrene and coronene at high pressure. Physics of the Earth and Planetary Interiors, 270: 29-39.

Connolly, J.A.D., 1990. Multivariable phase diagrams; an algorithm based on generalized thermodynamics. American Journal of Science, 290: 666-718.

Deng, L., Fei, Y., Liu, X., Gong, Z., Shahar, A., 2013. Effect of carbon, sulfur and silicon on iron melting at high pressure: Implications for composition and evolution of the planetary terrestrial cores. Geochimica et Cosmochimica Acta, 114: 220-233.

Derenne, S., Robert, F., 2010. Model of molecular structure of the insoluble organic matter isolated from Murchison meteorite. Meteoritics & Planetary Science, 45: 1461-1475.

Fei, Y., Bertka, C.M., Finger, L.W., 1997. High-Pressure Iron-Sulfur Compound, Fe3S2, and Melting Relations in the Fe-FeS System. Science, 275: 1621-1623.

Fortes, A.D., 2012. Titan's internal structure and the evolutionary consequences. Planetary and Space Science, 60: 10-17.

Franklin, R.E., 1949. A study of the fine structure of carbonaceous solids by measurements of true and apparent densities. Part II.—carbonized coals. Transactions of the Faraday Society, 45: 668-682.

Fulle, M. et al., 2016. Comet 67P/Churyumov–Gerasimenko preserved the pebbles that formed planetesimals. Monthly Notices of the Royal Astronomical Society, 462: S132-S137.

Grasset, O. et al., 2013. JUpiter ICy moons Explorer (JUICE): An ESA mission to orbit Ganymede and to characterise the Jupiter system. Planetary and Space Science, 78: 1-21.

Hilairet, N., Daniel, I., Reynard, B., 2006. Equation of state of antigorite, stability field of serpentines, and seismicity in subduction zones. Geophysical Research Letters, 33: L02302.

Holland, T.J.B., Powell, R., 1998. An internally consistent thermodynamic data set for phases of petrological interest. Journal of Metamorphic Geology, 16: 309-343.

Hyman, M., Rowe, M.W., 1983. Magnetite in CI chondrites. Journal of Geophysical Research, 88: A736.

Iess, L. et al., 2012. The tides of Titan. Science, 337: 457-9.

Kalousová, K., Sotin, C., 2018. Melting in High-Pressure Ice Layers of Large Ocean Worlds—Implications for Volatiles Transport. Geophysical Research Letters, 45: 8096-8103.

King, A.J., Schofield, P.F., Howard, K.T., Russell, S.S., 2015. Modal mineralogy of CI and CI-like chondrites by X-ray diffraction. Geochimica et Cosmochimica Acta, 165: 148-160.

Kivelson, M.G. et al., 1996. Discovery of Ganymede's magnetic field by the Galileo spacecraft. Nature, 384: 537-541.

Kivelson, M.G., Khurana, K.K., Volwerk, M., 2002. The Permanent and Inductive Magnetic Moments of Ganymede. Icarus, 157: 507-522.

Lellouch, E., Schmitt, B., Coustenis, A., Cuby, J.G., 2004. Titan's 5-micron lightcurve. Icarus, 168: 209-214.

Lodders, K., 2003. Solar System Abundances and Condensation Temperatures of the Elements. The Astrophysical Journal, 591: 1220-1247.

Lorenz, R.D. et al., 2019. Titan Seismology with Dragonfly : Probing the Internal Structure of the Most Accessible Ocean World, 50th Lunar and Planetary Science Conference, Houston, pp. 2173.

Malvoisin, B., Brunet, F., Carlut, J., Roumejon, S., Cannat, M., 2012. Serpentinization of oceanic peridotites: 2. Kinetics and processes of San Carlos olivine hydrothermal alteration. Journal of Geophysical Research-Solid Earth, 117: B04102.

Marchi, S. et al., 2019. An aqueously altered carbon-rich Ceres. Nature Astronomy, 3: 140-145.

McKinnon, W.B. et al., 2017. Origin of the Pluto–Charon system: Constraints from the New Horizons flyby. Icarus, 287: 2-11.

Morard, G. et al., 2018. Liquid properties in the Fe-FeS system under moderate pressure: Tool box to model small planetary cores. American Mineralogist, 103: 1770-1779.

Mousis, O. et al., 2009. A primordial origin for the atmospheric methane of Saturn’s moon Titan. Icarus, 204: 749-751.

Mueller, S., McKinnon, W.B., 1988. Three-layered models of Ganymede and Callisto: Compositions, structures, and aspects of evolution. Icarus, 76: 437-464.

Padron-Navarta, J.A. et al., 2013. Tschermak's substitution in antigorite and consequences for phase relations and water liberation in high-grade serpentinites. Lithos, 178: 186-196.

Quirico, E. et al., 2009. Precursor and metamorphic condition effects on Raman spectra of poorly ordered carbonaceous matter in chondrites and coals. Earth and Planetary Science Letters, 287: 185-193.

Schreyer, W., Abraham, K., Kulke, H., 1980. Natural sodium phlogopite coexisting with potassium phlogopite and sodian aluminian talc in a metamorphic evaporite sequence from Derrag, Tell Atlas, Algeria. Contributions to Mineralogy and Petrology, 74: 223-233.

Schubert, G., Stevenson, D.J., Ellsworth, K., 1981. Internal structures of the Galilean satellites. Icarus, 47: 46-59.

Schubert, G., Zhang, K., Kivelson, M.G., Anderson, J.D., 1996. The magnetic field and internal structure of Ganymede. Nature, 384: 544-545.

Scott, H.P., Williams, Q., Ryerson, F.J., 2002. Experimental Constraints on the Chemical Evolution of Icy Satellites. Earth and Planetary Science Letters, 203: 399-412.

Sohl, F., Spohn, T., Breuer, D., Nagel, K., 2002. Implications from Galileo Observations on the Interior Structure and Chemistry of the Galilean Satellites. Icarus, 157: 104-119.

Sotin, C. et al., 2018. Titan's interior structure after Cassini/Huygens, European Planetary Science Congress. EGU, pp. EPSC2018-1203.

Stofan, E.R. et al., 2007. The lakes of Titan. Nature, 445: 61-4.

Tobie, G., Lunine, J.I., Sotin, C., 2006. Episodic outgassing as the origin of atmospheric methane on Titan. Nature, 440: 61-64.

Urakawa, S. et al., 2004. Phase relationships and equations of state for FeS at high pressures temperatures and implications for the internal structure of Mars. Physics of the Earth and Planetary Interiors, 143: 469-479.

Vance, S., Bouffard, M., Choukroun, M., Sotin, C., 2014. Ganymede's internal structure including thermodynamics of magnesium sulfate oceans in contact with ice. Planetary and Space Science, 96: 62-70.

Vitale Brovarone, A. et al., 2017. Massive production of abiotic methane during subduction evidenced in metamorphosed ophicarbonates from the Italian Alps. Nature Communications, 8: 14134.

Wasson, J.T., Kallemeyn, G.W., 1988. Composition of Chondrites. Philosophical Transactions of the Royal Society of London. Series A, Mathematical and Physical Sciences, 325: 535-544.

Zimmer, C., Khurana, K.K., Kivelson, M.G., 2000. Subsurface Oceans on Europa and Callisto: Constraints from Galileo Magnetometer Observations. Icarus, 147: 329-347.

Figure captions

Fig. 1. Phase diagram for composition models 1 and 2. The grey area shows the major dehydration interval, lines correspond to major mineral reactions. The gray area is the dehydration zone that marks the transition between essentially hydrated mineral assemblage at low temperature and essentially anhydrous mineral assemblage at high temperature. Model 1 has a broader and lower temperature dehydration zone than model 2. Amph: amphibole, Atg: antigorite, Br: Brucite, Chl: chlorite, Cpx: clinopyroxene, Gt: garnet, NaPh: Na-phlogopite, Ol: olivine, Opx: orthopyroxene.

Fig. 2. Phase proportions in models 1 and 2 and for three isobars (fixed pressure and varying temperature). The magnesium-rich model 2 favors the formation of antigorite in the hydrous part of the diagram at the expense of chlorite, and the formation of orthopyroxene in the anhydrous part at the expense of olivine, with respect to model 1. Amph: amphibole, Atg: antigorite, Br: Brucite, Chl: chlorite, Cpx: clinopyroxene, Gt: garnet, NaPh: Na-phlogopite, Ol: olivine, Opx: orthopyroxene, Tlc: talc.

Fig. 3. Water content of the rock as a function of the temperature for model 1 (green curve for a silicate-FeS core; blue curve for the silicate fraction only) and model 2 (red curve) at 3 GPa.

Fig. 4. Raman spectra of Na-phlogopite from the experiments (Run 2, blue curve) compared to a reference spectrum (K-phlogopite R040144 from the RRUFF database http://rruff.info, red curve). The grey vertical lines at frequencies of the main vibration modes of phlogopite show the match between the reference spectrum and the one obtained on the present experiment. The two intense peaks in the 1200-1800 cm^{-1} region correspond

to the vibrational modes of amorphous carbon, a result of the transformation of the paraffin wax and pyridine analogs of organic matter. Aliphatic signature in the 2700-3200 cm^{-1} region is due to the resin used to consolidate the sample.

Fig. 5. Density profiles of the silicate fraction for model 1 (blue curve) and model 2 (red curve), and density profile of the silicate-sulfide mixture for model 1 (green curve). (a.) Isotherms 300 K (dashed lines) and 1300 K (solid lines). (b.) Isobar 3 GPa. Dehydration of hydrous minerals to denser dry minerals results in a progressive increase in density with increasing temperature.

Fig. 6. Models of interior structures for Titan and Ganymede. CM: carbonaceous matter required for matching the density and MoI with a density of 1400 kg/m^3 in Titan and 1800 kg/m^3 in Ganymede.

Fig. 7. Mass vs. MoI relationship for Titan and Ganymede for a range of core radii and compositions. Empty symbols and dashed curves: CI chondrite composition with ice-silicate-iron sulfide mixture and fixed radius. Large filled circles: data for Ganymede (blue) and Titan (orange). Effect of non-hydrostaticity (NH) on Titan MoI determination is shown. Small circles: effect of different mass fractions (given in wt%) of carbonaceous matter assuming constant average densities in each layer. Small arrows indicate the effect of neglecting compressibility in these models.

Tables

Table 1. Composition of the bulk and silicate fraction of the core in models 1 and 2 assuming a CI chondrite precursor (Wasson & Kallemeyn 1988).

Oxide/sulfide (wt.%)	Undifferentiated	Silicate fraction Model 1	Silicate fraction Model 2
MgO	22.85	29.67	36.03
SiO_2	31.91	41.43	50.31
CaO	1.83	2.37	2.88
Na_2O	0.92	1.19	1.45
Al_2O_3	2.31	3.00	3.64
FeO	17.21	22.35	5.69
FeS	22.98	-	-

Table 2. Starting conditions for MoI calculations displayed in Fig. 7. Radii of the layers and at interfaces are given in km. X is the mass fraction of carbonaceous matter added to the core to match the total mass of the moon.

Titan					with carbonaceous matter density of 1400 kg/m^3		
R surface	R crust/ocean	R ocean/HP ice	Rcore		Rcore		X
2575	2499	2105	1800		1800		0.06
2575	2499	2105	1900		1900		0.13
2575	2499	2105	2000		2000		0.20
2575	2499	2105	2100		2100		0.26
2575	2499		2200		2200		0.32
Ganymede					with carbonaceous matter density of 1800 kg/m^3		
R surface	R crust/ocean	R ocean/HP ice	R ice/silicate	R Fe-FeS core	R silicate	R Fe-FeS core	X
2631	2539	2193	1800	1080	1800	1055	0.02
2631	2539	2193	1900	1140	1900	1035	0.09
2631	2539	2193	2000	1200	2000	1012	0.16
2631	2539	2193	2100	1260	2100	984	0.23
2631	2539		2200	1320	2200	952	0.29

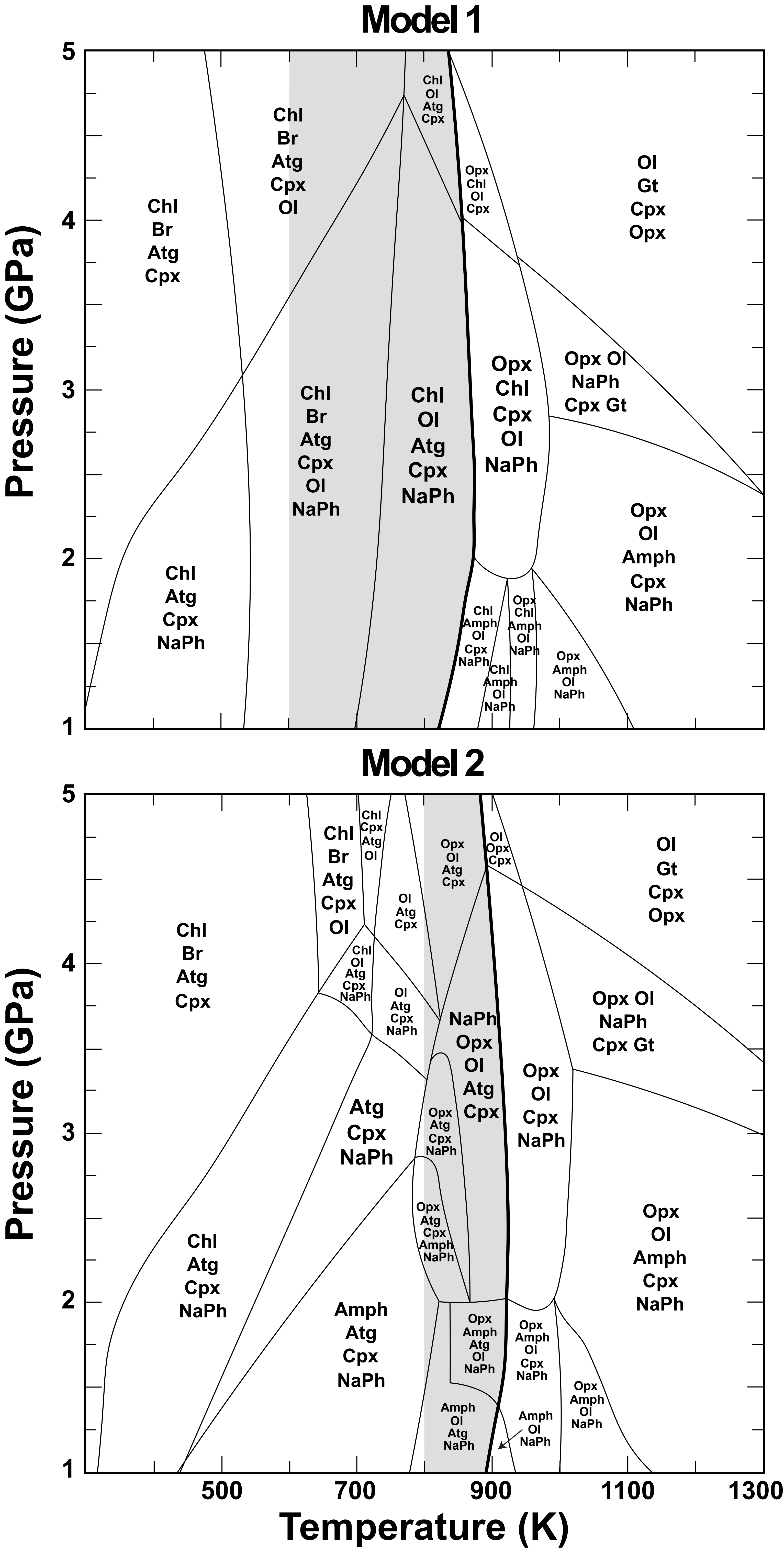
Model 1
Pressure (GPa)
5
4
3
2
1
Chl Br Atg Cpx
Chl Br Atg Cpx Ol
Chl Ol Atg Cpx
Opx Chl Ol Cpx
Ol Gt Cpx Opx
Chl Br Atg Cpx Ol NaPh
Chl Ol Atg Cpx NaPh
Opx Chl Cpx Ol NaPh
Opx Ol NaPh Cpx Gt
Opx Ol Amph Cpx NaPh
Chl Atg Cpx NaPh
Chl Amph Ol Cpx NaPh
Opx Chl Amph Ol NaPh
Chl Amph Ol NaPh
Opx Amph Ol NaPh
Model 2
Pressure (GPa)
5
4
3
2
1
Chl Br Atg Cpx Ol
Chl Cpx Atg Ol
Opx Ol Atg Cpx
Ol Opx Cpx
Ol Gt Cpx Opx
Ol Atg Cpx
Chl Br Atg Cpx
Chl Ol Atg Cpx NaPh
Ol Atg Cpx NaPh
NaPh Opx Ol Atg Cpx
Opx Ol NaPh Cpx Gt
Opx Ol Cpx NaPh
Atg Cpx NaPh
Opx Atg Cpx NaPh
Opx Atg Cpx Amph NaPh
Chl Atg Cpx NaPh
Opx Ol Amph Cpx NaPh
Amph Atg Cpx NaPh
Opx Amph Atg Ol NaPh
Opx Amph Ol Cpx NaPh
Opx Amph Ol NaPh
Amph Ol Atg NaPh
Amph Ol NaPh
500
700
900
1100
1300
Temperature (K)

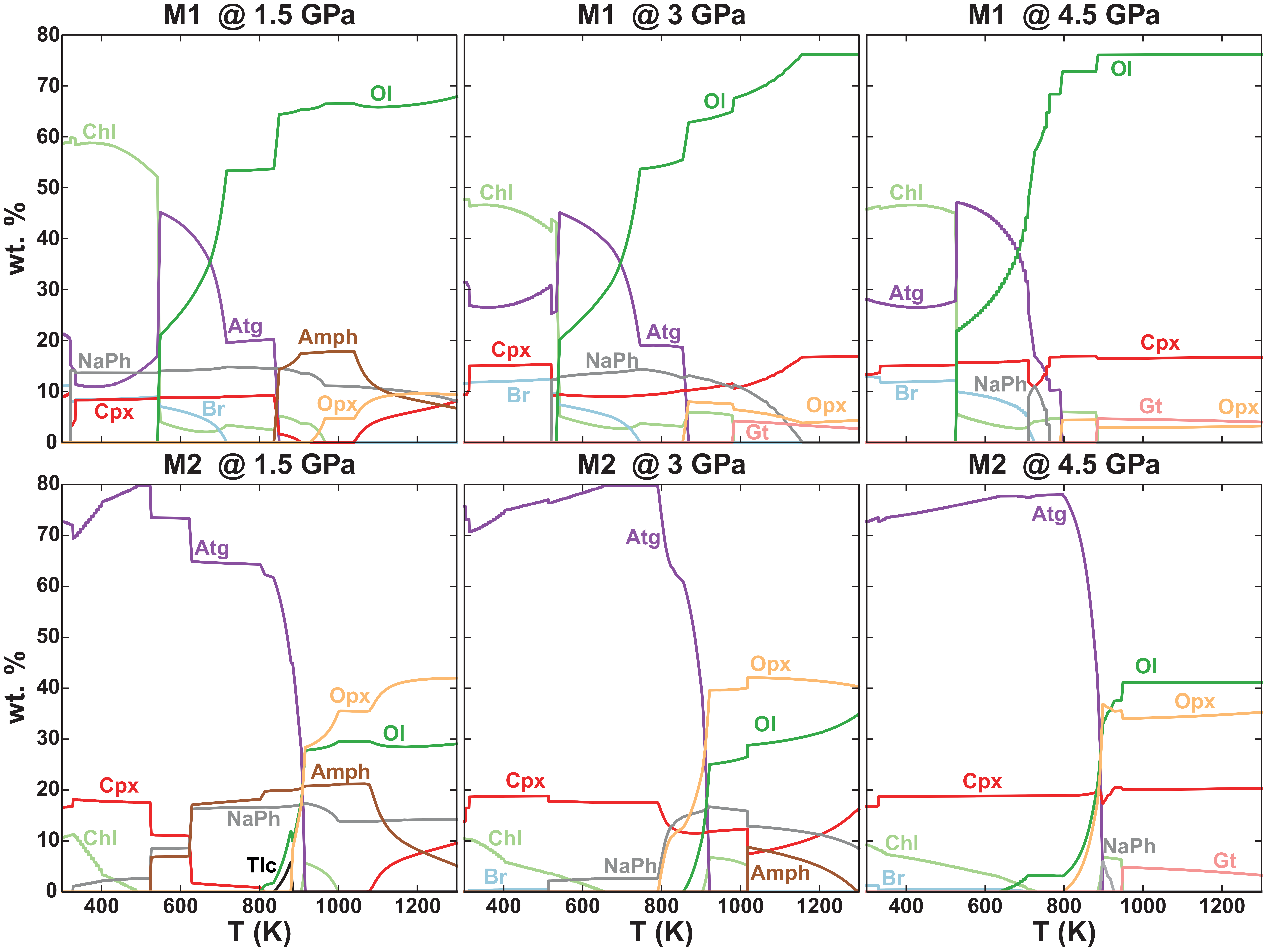
M1 @ 1.5 GPa
M1 @ 3 GPa
M1 @ 4.5 GPa
M2 @ 1.5 GPa
M2 @ 3 GPa
M2 @ 4.5 GPa
wt. %
T (K)
0
10
20
30
40
50
60
70
80
400
600
800
1000
1200
Ol
Chl
Atg
Cpx
NaPh
Br
Amph
Opx
Gt
Tlc

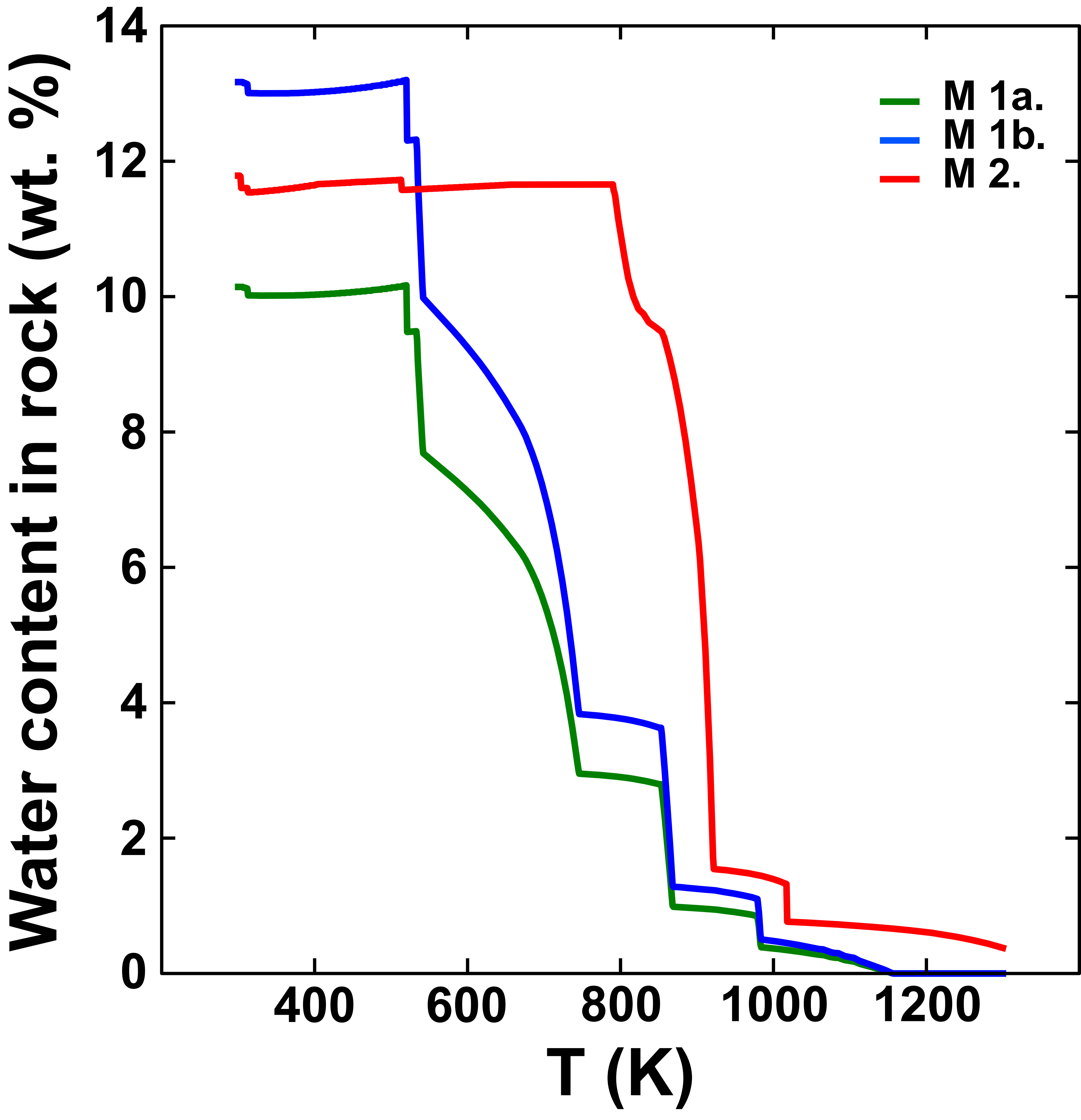
Water content in rock (wt. %)
0
2
4
6
8
10
12
14
400
600
800
1000
1200
T (K)
M 1a.
M 1b.
M 2.

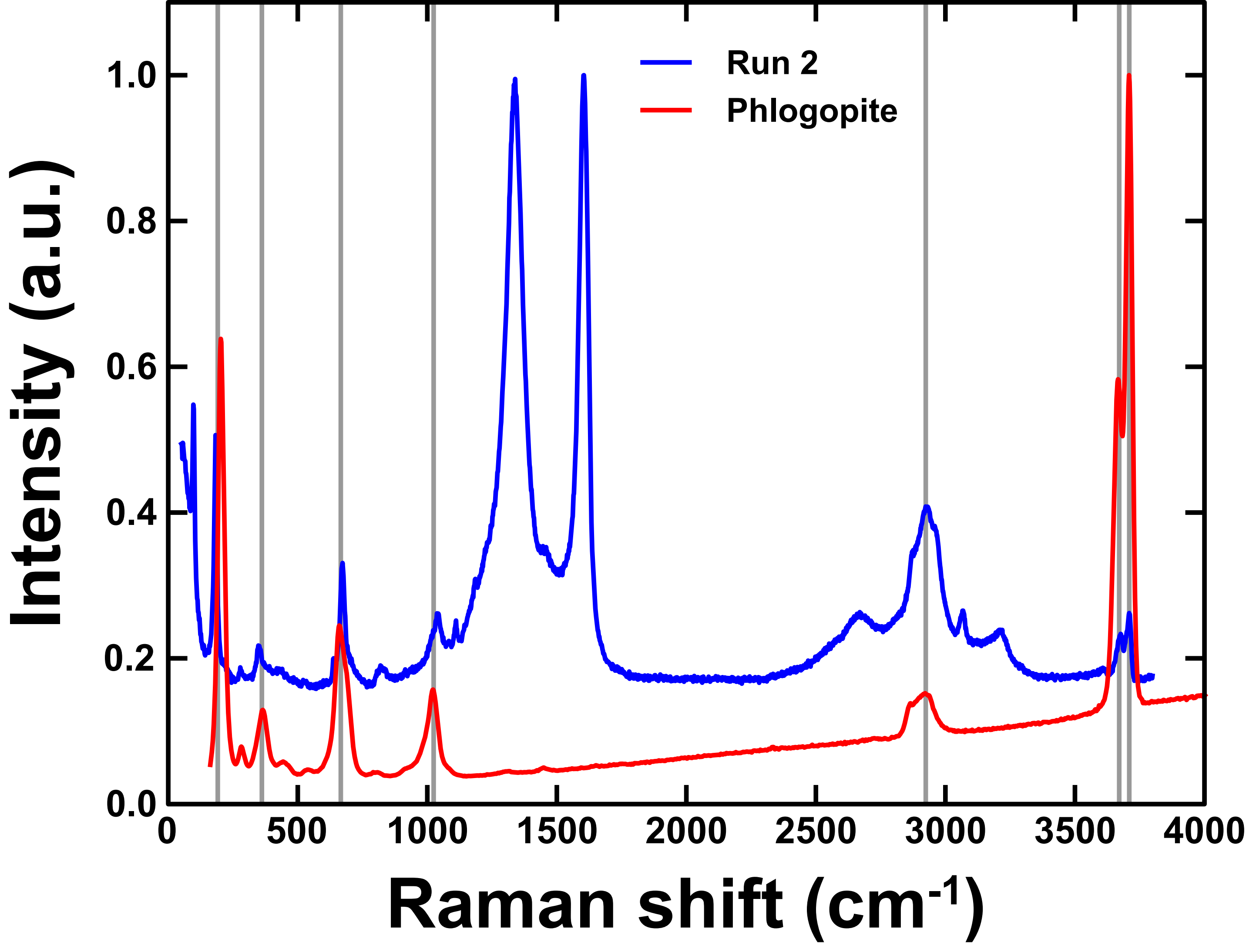
Run 2
Phlogopite
Intensity (a.u.)
Raman shift (cm^{-1})
0.0
0.2
0.4
0.6
0.8
1.0
0
500
1000
1500
2000
2500
3000
3500
4000

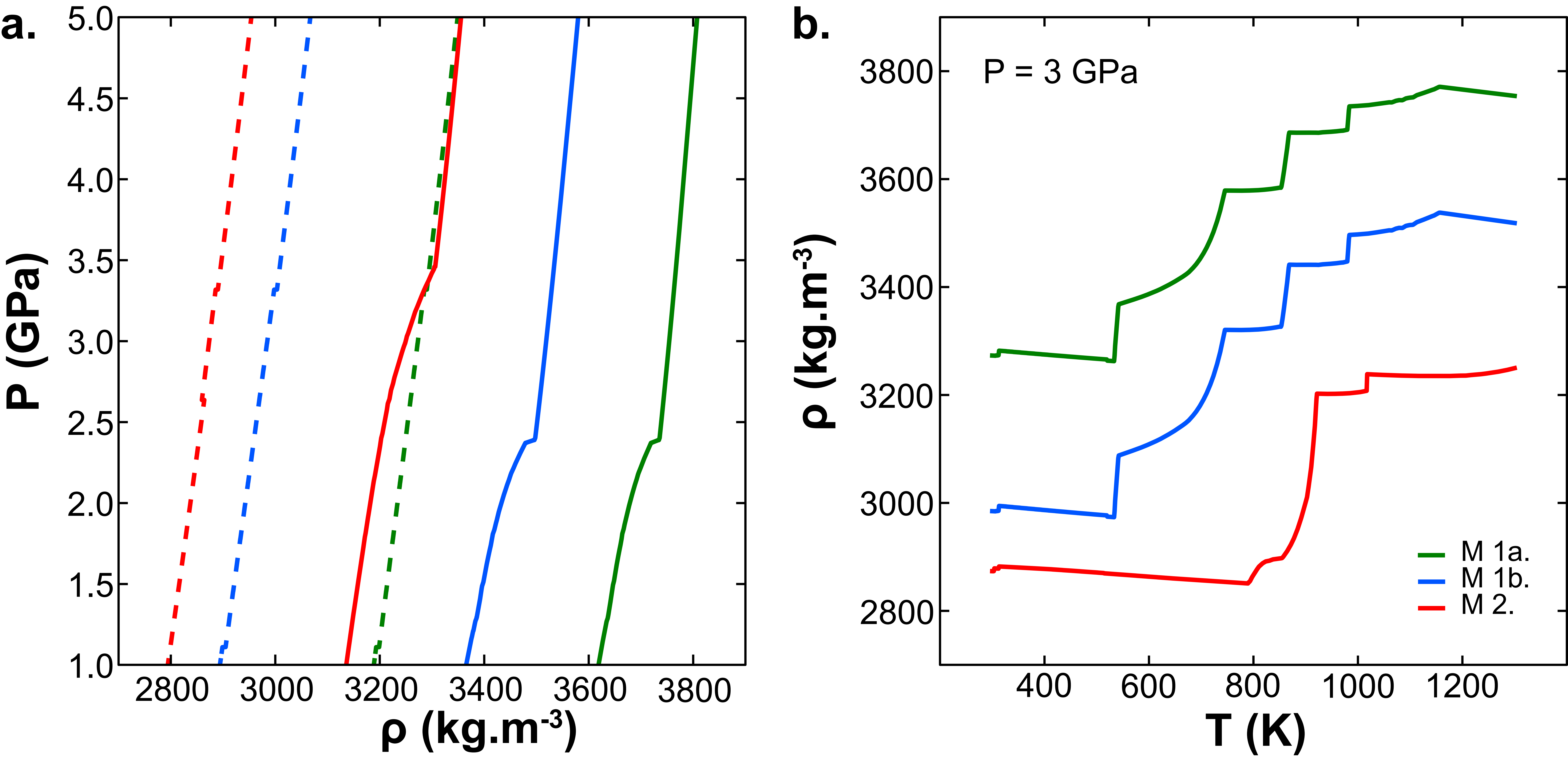
a.
P (GPa)
5.0
4.5
4.0
3.5
3.0
2.5
2.0
1.5
1.0
2800
3000
3200
3400
3600
3800
ρ (kg.m-3)
b.
P = 3 GPa
ρ (kg.m-3)
3800
3600
3400
3200
3000
2800
400
600
800
1000
1200
T (K)
M 1a.
M 1b.
M 2.

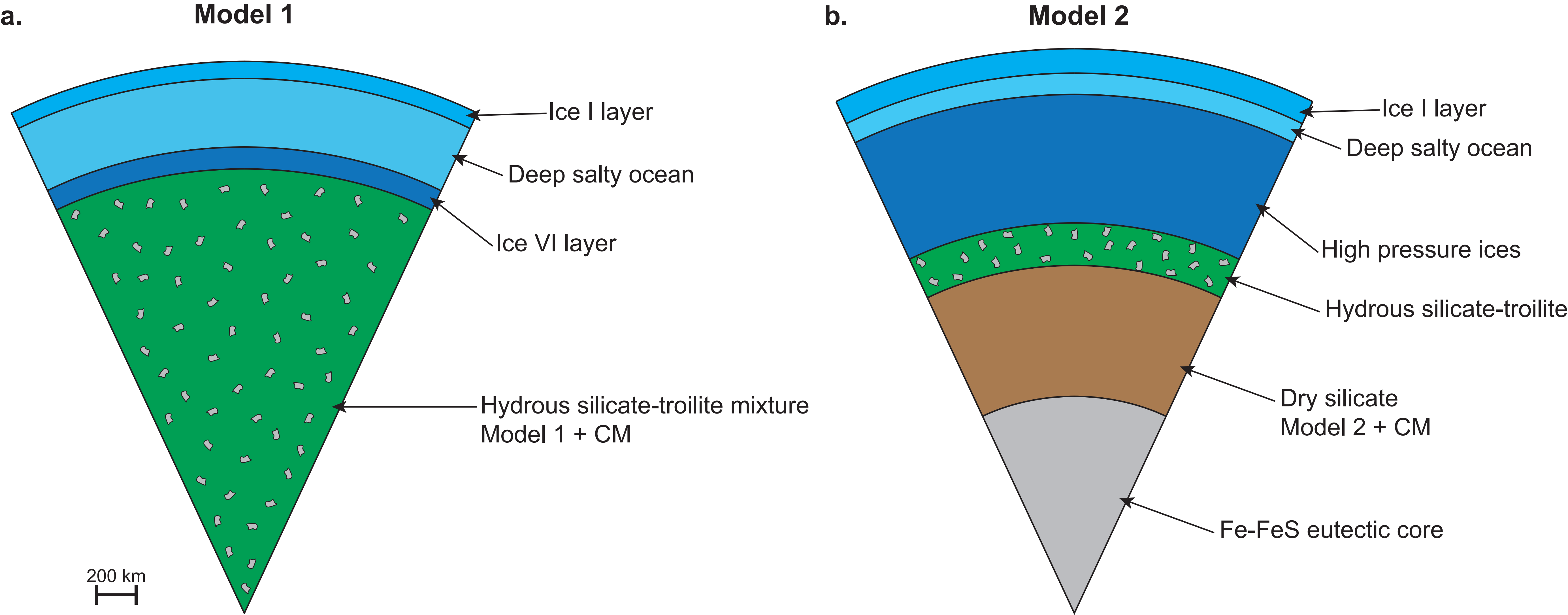
a.
Model 1
Ice I layer
Deep salty ocean
Ice VI layer
Hydrous silicate-troilite mixture
Model 1 + CM
200 km
b.
Model 2
Ice I layer
Deep salty ocean
High pressure ices
Hydrous silicate-troilite
Dry silicate
Model 2 + CM
Fe-FeS eutectic core

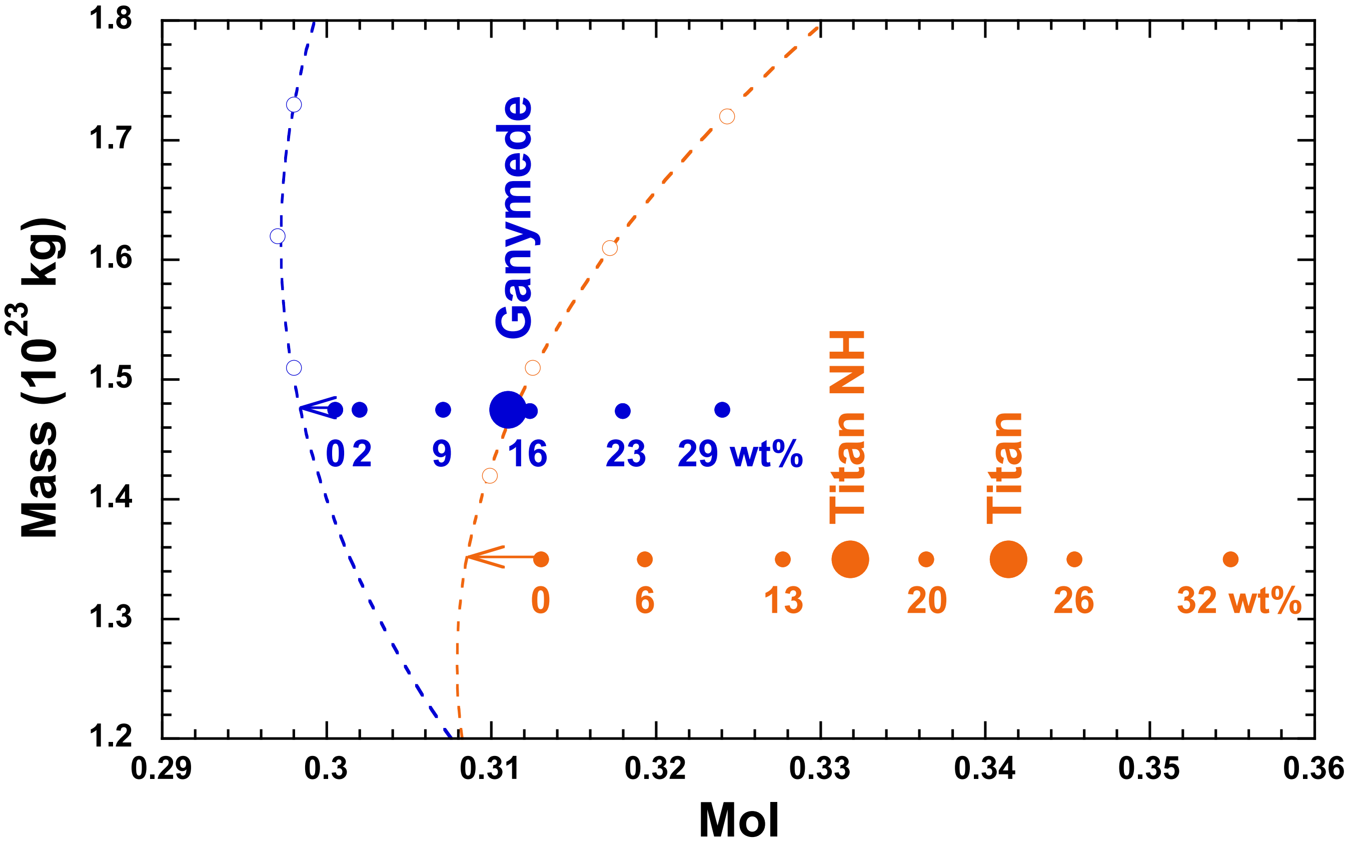

1.8
1.7
1.6
1.5
1.4
1.3
1.2
Mass (10^{23} kg)
0.29
0.3
0.31
0.32
0.33
0.34
0.35
0.36
MoI
Ganymede
0 2
9
16
23
29 wt%
Titan NH
Titan
0
6
13
20
26
32 wt%